Canonical foliations of neural networks: application to robustness

Eliot Tron, Nicolas Couellan, Stéphane Puechmorel

Canonical foliations of neural networks: application to robustness

Eliot Tron ELIOT.TRON@ENAC.FR
ENAC,
7 Avenue Edouard Belin, 31400 Toulouse, France

Nicolas Couellan NICOLAS.COUELLAN@RECHERCHE.ENAC.FR
ENAC, Université de Toulouse,
7 Avenue Edouard Belin, 31400 Toulouse, France

Stéphane Puechmorel STEPHANE.PUECHMOREL@ENAC.FR
ENAC, Université de Toulouse,
7 Avenue Edouard Belin, 31400 Toulouse, France

Abstract

Deep learning models are known to be vulnerable to adversarial attacks. Adversarial learning is therefore becoming a crucial task. We propose a new vision on neural network robustness using Riemannian geometry and foliation theory. The idea is illustrated by creating a new adversarial attack that takes into account the curvature of the data space. This new adversarial attack called the *two-step spectral attack* is a piece-wise linear approximation of a geodesic in the data space. The data space is treated as a (degenerate) Riemannian manifold equipped with the pullback of the Fisher Information Metric (FIM) of the neural network. In most cases, this metric is only semi-definite and its kernel becomes a central object to study. A canonical foliation is derived from this kernel. The curvature of transverse leaves gives the appropriate correction to get a two-step approximation of the geodesic and hence a new efficient adversarial attack. The method is first illustrated on a 2D toy example in order to visualize the neural network foliation and the corresponding attacks. Next, experiments on the `MNIST` dataset with the proposed technique and a state of the art attack presented in Zhao et al. (2019) are reported. The result show that the proposed attack is more efficient at all levels of available budget for the attack (norm of the attack), confirming that the curvature of the transverse neural network FIM foliation plays an important role in the robustness of neural networks.

Keywords: Neural Networks, Robustness, Fisher Information Metric, Information geometry, Adversarial attacks.

1. Introduction

Lately there has been a growing interest in the analysis of neural network robustness and the sensitivity of such models to input perturbations (Fawzi et al. (2018b); Shaham et al. (2018); Kolter and Wong (2018); Raghunathan et al. (2020)). Most of these investigations have highlighted their weakness to handle adversarial attacks (Szegedy et al. (2014)) and have proposed some means to increase their robustness. Adversarial attacks are real threats that could slow down or eventually stop the development of neural network models or their applications in contexts where robustness guarantees are needed. For example, in the specific case of aviation safety, immunization of critical systems to adversarial attacks should not

only be guaranteed but also certified. Therefore, addressing the robustness of future onboard or air traffic control automated systems based on such models is a main concern.

Adversarial attacks are designed to fool classification models by introducing perturbations in the input data. These perturbations remain small and in the case of images for example, may be undetectable to the human eye. So far, most of the research effort has focused on designing such attacks in order to augment the training dataset with the constructed adversarial samples and expecting that training will be more robust. Among these methods, one can refer to the Fast Gradient Sign methods (Goodfellow et al. (2015)), robust optimization methods (Madry et al. (2019)), DeepFool (Moosavi-Dezfooli et al. (2016)), and others (Fawzi et al. (2017)). There are major drawbacks with these approaches. Most attacks are data dependent and provide no guarantees that all relevant attacks have been considered and added to the training set. Furthermore, training in such manner does not acquire a global knowledge about the weakness of the model towards adversarial threats. It will only gain robustness for attacks that have been added to the dataset. However, crafting adversarial attacks by exploiting the properties of neural network learning is useful to understand the principles at play in the robustness or sensitivity of neural architectures.

Many authors consider neural network attacks and robustness properties in a Euclidean input space. Yet, it is commonly admitted that to learn from high dimensional data, data must lie in a low dimensional manifold (Fefferman et al. (2016)). Such manifold has in general non-zero curvature and Riemannian geometry should therefore be a more appropriate setting to analyze distances and sensitivity from an attack point of view. Furthermore, to analyze neural network model separation capabilities and its robustness, it is critical to understand not only the topology of the decision boundaries in the input space but also the topology of iso-information regions induced by the neural network. Again, there is no reason to believe that these sub-manifolds have zero curvature in general. The Fisher information metric (FIM) is a valid metric for such purpose. Indeed, the network output is seen as a discrete probability that lies on a statistical manifold. The FIM may then be used as a Riemannian metric at the output and the pullback metric of the Fisher information as a metric for the input manifold (Zhao et al. (2019)). The importance of the FIM in the context of deep neural networks has already been pointed out by several authors. In Karakida et al. (2019), it is shown that the FIM defines the landscape of the parameter space and the maximum FIM eigenvalue defines an approximation of the appropriate learning rate for gradient methods. The FIM with respect to data (also called local data matrix) instead of network parameters has also been investigated from a geometric perspective in Grementieri and Fioresi (2021). The authors have shown that training data are organized on submanifolds (leaves) of a foliation of the data domain. A few authors have also tried to exploit this geometric knowledge to construct adversarial attacks or get some form of immunization from them. In Zhao et al. (2019), the direction of eigenvector corresponding to the maximum eigenvalue of the pullback FIM metric is used as a direction of attack where as in Shen et al. (2019), similar developments are proposed to robustify the model by regularizing the neural network loss function by the trace of the FIM. More specifically, in Zhao et al. (2019), the authors have shown that the one step spectral attack (OSSA) they proposed is more efficient than the Fast Gradient Sign and the One Step Target Class methods Kurakin et al. (2016). In this work, we build on the work of Zhao et al. (2019) and exploit further the geometrical properties of the foliation of the pullback metric of the neural network FIM. More specifically,

we show that the curvature of the leaf of the transverse foliation can be utilized to construct a two-step attack procedure referred as *two-step* attack. Given a budget of attack, meaning the Euclidean norm of the attack vector, we first move in the direction of the eigenvector corresponding to the maximum eigenvalue of the FIM as proposed in Zhao et al. (2019) and then make another move that takes into account the curvature. The two steps could be seen as a discretized move along a geodesic curve. The interest of this procedure is not only to prove that, for a given budget of attack, it is possible to construct worse attacks than those proposed in Zhao et al. (2019) but also and more importantly to emphasize the role of curvature in the sensitivity of neural network models. Mathematically, this translates into the expression of the quadratic form approaching the Kullback-Leibler divergence between the network output probability distribution at the origin of the attack and the probability distribution at the point reached by the attack. Indeed, we show that this expression makes explicit use of the Riemannian curvature tensor of the foliation in the input space. To better grasp and visualize the effect of curvature on the attacks, we provide details on the calculation of the neural network FIM and the corresponding attacks on a `XOR` toy problem. The small dimension of the problem allows also 2D illustrations of the phenomenon. To demonstrate experimentally the benefit of exploiting the foliation curvature, experiments are conducted first with the `XOR` toy problem and next with the `MNIST` (Deng (2012)) dataset. The fooling rate that computes the percentage of wrong prediction when attacks are making use of the curvature is exploited on random data points in comparison to attacks that are not taking the curvature into account. The result show a substantial increase for the fooling rates when curvature is utilized.

The contribution of this study is two-fold: It proposes a Riemannian geometry framework for analyzing the robustness of neural networks but also provides a two-step procedure for crafting adversarial attacks that have proven to be more effective than state of the art attacks. These attacks may later be used as an immunization mechanism for training the network.

The paper is organized as follows. Section 2 details the general mathematical framework of this study and defines precisely the adversarial attacks that are considered. In the first part of Section 3, the construction of the local attack by Zhao et al. (2019) is recalled. Next, in Section 4, the main developments of this research are detailed, consisting in extending the local attack using the geometry of the problem resulting in the so-called two-step attack. Section 5 is dedicated to the illustration of the method through a simple play-test problem. It details more precisely the required calculations on a simple low dimensional problem and provides illustrations of the resulting foliation at the heart of the technique. Section 6 provides the numerical results and Section 7 concludes the article. Appendices A and B recall some important concepts of Riemannian geometry that are used throughout the article.

2. Problem statement

2.1 Setup

In this paper, we are studying the behavior of a neural network $N : \mathcal{X} \to \mathcal{M}$. Its output can be considered as a parameterized probability density function $p_\theta(y \mid x) \in \mathcal{M}$ where $\mathcal{M}$ is a manifold of such probability density functions, $x \in \mathcal{X}$ is the input, $y \in \mathcal{Y}$ is the targeted label and $\theta \in \Theta$ is the parameter of the model (for instance the weights and biases in a

perceptron). The geometric study of such probability distributions is part of *Information Geometry* Nielsen (2020).

In this case, $\mathcal{M}$ and $\mathcal{X}$ are two (degenerate) Riemannian Manifolds when equipped with the *Fisher Information Metric* (FIM). Fisher Information is originally a way to measure the variance of a distribution along a parameter. It was used as a Riemannian metric by Jeffrey and Rao (1945-1946), then by Amari, which gave birth to *Information Geometry* Amari (2016); Nielsen (2020). Measuring how the distribution of the predicted labels changes with input perturbations falls exactly in our usecase. This explains why the FIM is a good candidate to be $\mathcal{X}$ and $\mathcal{M}$'s metric.

Definition 1 (Fisher Information Metric) *The Fisher Information Metric (FIM) on the manifold $\mathcal{X}$ at the point x is defined by the following positive semi-definite symmetric matrix:*

$$g_{ij}(x) = \mathbb{E}_{y|x,\theta}\left[\partial_{x_i} \ln p(y \mid x, \theta) \partial_{x_j} \ln p(y \mid x, \theta)\right].$$

Remark 1 *Note that this definition is not the usual definition of the Fisher Information. Indeed, the one defined by Fisher, used in the work of Amari and many others, differentiate with respect to the parameter θ where we differentiate with respect to the input x. The authors in Grementieri and Fioresi (2021) call this new metric the* local data matrix *to avoid confusion.*

It is important to notice that for the probability distribution given by a neural network, the Fisher Information is only a degenerate Riemmannian metric, meaning that the matrix $G = (g_{ij})_{i,j}$ is not full rank. This is mainly due to the fact that $\dim \mathcal{X} \gg \dim \mathcal{M}$ in most cases of neural networks classifiers.

In this generate Riemmannian geometric setting, one can define the kernel of the metric at each point. This subset of the tangent space $T\mathcal{X}$ is called a distribution and it is integrable under some assumptions, meaning that it gives rise to a *foliation* i.e. a partition of $\mathcal{X}$ into submanifolds called *leaves*. With this canonical foliation, a dual one can be defined using the orthogonal[1] complement of the kernel at each point. It is called the *transverse* foliation. At each point, moving along the FIM kernel leaf will not modify the output of the neural network. The properties of the transverse foliation will thus be of great interest in the setting of adversarial attacks. The reader may find more details on these geometric objects in the appendix A and B.

2.2 Adversarial attacks

One primary goal of this article is to craft the best *adversarial attack* possible, or at least approach it. An adversarial attack aims at disturbing the output of the neural network by adding noise to the original input, with the intention of changing the predicted class and thus fooling the network. The FIM with respect to the input is a good measure of dissimilarity between outputs, given a displacement of the input. In order to change the predicted class after the attack one would want to maximize the dissimilarity between the predicted distribution of probability before and after the attack. In other words, one would

1. Orthogonal with respect to the ambiant Euclidean metric.

like to maximize the FIM's geodesic distance[2] $d(x_o, x_a)$ between the input point x_o and the point x_a after the attack.

Proposition 2.1 *The geodesic distance can be expressed with the Riemannian norm and the logarithm map[3]:*

$$d(x_o, x_a)^2 = \left\|\log_{x_o} x_a\right\|_{\mathcal{X}}^2 = g_{x_o}\left(\log_{x_o} x_a, \log_{x_o} x_a\right).$$

Otherwise said, if $v = \log_{x_o} x_a$ is the initial velocity of the geodesic between the two points,

$$d(x_o, \exp_{x_o}(v))^2 = \|v\|_{\mathcal{X}}^2.$$

The optimal solution will thus be the $\hat{x}_a$ maximizing this quantity, with some constraints. Indeed, one of the characteristics of a good adversarial attack is to be as undetectable as possible by usual measurements on the input. A usual measure for that is the Euclidean distance between x_o and x_a. The attacked point will thus be constrained to the Euclidean ball of given (small) radius and centered at x_o. The optimal attacked point is the result of a geodesic move from x_o with initial velocity $v \in T_{x_o}\mathcal{X}$.

Definition 2 (ε-Adversarial Attack Problem) *The optimal geodesic attack with a Euclidean budget of $\varepsilon > 0$ and initial velocity v verifies:*

$$\max_{v \in T_{x_o}\mathcal{X}} \|v\|_{\mathcal{X}}^2 \;\; \textit{subject to} \;\; \left\|\exp_{x_o}(v) - x_o\right\|_2^2 \leq \varepsilon^2 \qquad (\varepsilon\text{-AAP})$$

Remark 2 *Some other authors Fawzi et al. (2018a) are looking for the smallest attack in Euclidean norm that changes the predicted class. We are taking the problem in reverse and looking for an imperceptible attack with respect to a sensor with an activation level of ε (e.g. the human eye, the human ear, camera or some other devices) with no guarantees that there exists a class changing attack. However, in real life context where dimension is large, it has been shown that such class changing attacks exist for small ε with high probability Gilmer et al. (2018).*

A usual optimization algorithm could solve this problem, but the amount of calculus would be tremendous since the geodesic requires to solve an ODE with boundary conditions each time. This greedy solution is thus not feasible in practice. To get close to the optimal solution, the geodesic can be approximated by Euclidean steps.

3. A local method

The authors in Zhao et al. (2019) have proposed a method to approximate the solution of a near-(ε-AAP) problem. Their formulation of the Adversarial Attack Problem is not exactly the same though. The criteria they are maximizing is not the geodesic distance, but the Kullback-Leibler divergence. The matter with (KL) divergences is that they are not

2. see Definition 8 in A
3. see Definition 11 in A

distances, because often not symmetric. Nevertheless, if G is the matrix associated to the FIM, a second order Taylor approximation gives us that:

$$D_{KL}\left(p_\theta\left(y \mid x\right) \parallel p_\theta\left(y \mid x+v\right)\right) = \frac{1}{2} v^T G_x v + o\left(\|v\|^2\right)$$
$$= \frac{1}{2} g_x\left(v, v\right) + o\left(\|v\|^2\right) = \frac{1}{2}\|v\|_{\mathcal{X}}^2 + o\left(\|v\|^2\right).$$

Then, the Euclidean constraint is taken directly on v meaning that x_o is moved by a Euclidean step in the direction of v. The problem thus solved in Zhao et al. (2019) is a linear approximation of (ε-AAP). Doing so amounts to approaching the geodesic by its initial velocity. In other words, the first order approximation $\exp_{x_o}(v) \approx x_o + v$ is used for this section.

Proposition 3.1 *The vector $\hat{v}$ maximizing the quadratic form $v \mapsto v^T G_x v$ is an eigenvector of the FIM G_x corresponding to the largest eigenvalue. Its re-normalization by $\frac{\varepsilon^2}{\|\hat{v}\|_2^2}$ gives an approximated solution to (ε-AAP). This method is illustrated by Figure 1.*

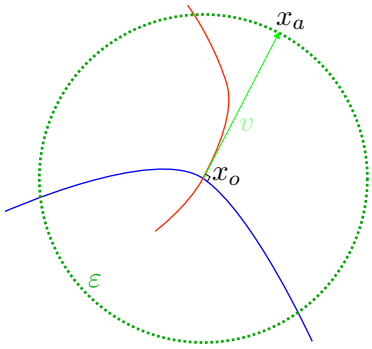

Figure 1: The one-step spectral attack in action. The circle represents the Euclidean budget. The blue curve represents the leaf of the kernel foliation and the red curve represents the transverse foliation.

Proof

To maximize this quadratic form under the constraint $\|v\|_2^2 = \varepsilon^2$, Karush-Kuhn-Tucker's optimality conditions[4] ensure that there exists a scalar $\lambda \in \mathbb{R}$ such that the optimum attack $\hat{v}$ satisfies:

$$\nabla_v\left(v^T G_x v\right) - \lambda \nabla_v\left(\|v\|_2^2 - \varepsilon^2\right) = 0$$
$$\implies \left(G_x + G_x^T\right)\hat{v} = \lambda 2\hat{v}$$
$$\implies G_x \hat{v} = \lambda \hat{v}.$$

Otherwise said, the optimum $\hat{v}$ is in the set of G_x's eigenvectors. In this case:

$$\|\hat{v}\|_{\mathcal{X}}^2 = \hat{v}^T G_x \hat{v} = \hat{v}^T \lambda \hat{v} = \lambda \|\hat{v}\|_2^2 = \lambda \varepsilon^2.$$

4. See H. W. Kuhn (1951) for more details.

Thus, $\hat{v}$ corresponding to the largest eigenvalue maximizes the Riemannian norm. ■

Remark 3 *The KKT optimality conditions lead to two valid and yet very different solutions: $\hat{v}$ and $-\hat{v}$. To choose between the two, we select the solution decreasing the probability of the original class the most, meaning that we select the attack vector $v \in \{\hat{v}, -\hat{v}\}$ satisfying:*

$$p_\theta\left(y_{x_o} \mid x_o - v\right) > p_\theta\left(y_{x_o} \mid x_o + v\right). \tag{1}$$

With this choice, we increase the probability of fooling the network on this point.

This first method is very local and does not take into account the curvature of the data. Hence, in regions of $\mathcal{X}$ where this curvature is high, we cannot rely on this method anymore.

4. A two-step attack

The idea here is to take a first local step v as in Section 3, and then take a second step to refine the linear approximation. The two-step nature of this attack allows the second step to take into account the curvature of the area around the input point. This method is able to exploit the geometry of the problem to construct a better approximation of the original problem (ε-AAP). This attack will be named the Two Step Spectral Attack (TSSA) .

Let v be the approximated solution of (ε-AAP) using the method of Section 3 but with a budget of $\mu^2 < \varepsilon^2$.

The new problem to solve is the following:

$$\max_w \|w\|_{\mathcal{X}}^2 \text{ subject to } \begin{cases} \|w+v\|_2^2 \leq \varepsilon^2 \\ \|v\|_2^2 = \mu^2 < \varepsilon^2 \\ v \text{ eigenvector of } G_x \end{cases} \tag{S2P}$$

One could solve this problem the same way as in Section 3 by taking w the eigenvector of G_{x+v} with the largest eigenvalue once again (see Figure 2). By doing that, we linearly approach the geodesic between x_o and x_a by two Euclidean lines. Taking more steps would approximate better the geodesic. Using only two steps as proposed is a simple procedure from a computational point of view and still achieves significantly better results than taking just one step as we will see in Section 5.

To explicit the action of the curvature at x of the input space on the trajectory of this multi-step attack, we will approximate G_{x+v} by its value at x using normal coordinates[5].

Remark 4 *In the sequel of the article, for any vector (or tensor) x, $\bar{x}$ will denote x expressed in terms of normal coordinates. Besides, we are going to use the Einstein summation notation omitting the symbol $\sum$ whenever the index over which the sum should apply repeats.*

Proposition 4.1 *If $\overline{x}$ are the normal coordinates at x_o and if R is the Riemannian curvature tensor, then*

$$w^T G_{x+v} w = \frac{\partial x^m}{\partial \overline{x}^i}\frac{\partial x^n}{\partial \overline{x}^j}\left(\delta_{mn} + \frac{1}{3}\overline{R}_{mkln}(x)\overline{v}^k\overline{v}^l\right) w^i w^j + o\left(\|v\|^2\right) \tag{2}$$

5. see Definition 10 in A

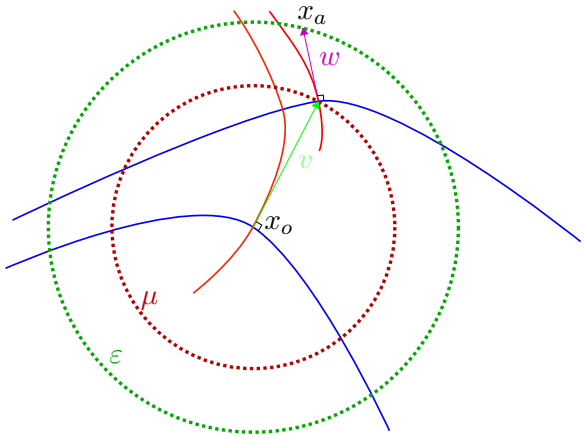

Figure 2: The two-step attack in action. The two circles represent the Euclidean budget. The blue curves represent the leaves of the kernel foliation and the red curves represent the transverse foliation.

Proof

$$\begin{aligned} w^T G_{x+v} w &= \left(G_{x+v}\right)_{ij} w^i w^j \\ &= \frac{\partial x^m}{\partial \overline{x}^i}\frac{\partial x^n}{\partial \overline{x}^j}\left(\overline{G}_{x+v}\right)_{nm} w^i w^j \\ &= \frac{\partial x^m}{\partial \overline{x}^i}\frac{\partial x^n}{\partial \overline{x}^j}\left(\delta_{mn} + \frac{1}{3}\overline{R}_{mkln}(x)\overline{v}^k\overline{v}^l + o\left(\|v\|^2\right)\right) w^i w^j. \end{aligned}$$

The last line is obtained by the second-order Taylor expansion of g in normal coordinates centered at x. The reader can find details of the computations in Willmore (2013), Section 3.5 Corollary 7. ■

Proposition 4.2 *By denoting* $\overline{w} = \left(\frac{\partial x^m}{\partial \overline{x}^i} w^i\right)_m = Pw$ *and* $R_v = \overline{R}_{mkln}(x)\overline{v}^k\overline{v}^l$, *Equation 2 can be rewritten with matrix notation by the following:*

$$\|w\|^2_{\mathcal{X}} = \|\overline{w}\|^2_2 + \frac{1}{3}\overline{w}^T R_v \overline{w} + o\left(\|v\|^2\right). \tag{3}$$

Remark 5 *In what follows,* $\|w\|^2_{\mathcal{X}}$ *will always be taken at* $x+v$, *and be approximated by the right hand of Equation 3. Additionally, we compare* w *and* v *without taking into account parallel transport since the Christoffel symbols vanish around the origin in normal coordinates.*

The transition matrix P is equal to $\left(\frac{\partial x^i}{\partial \overline{x}^j}\right)_{i,j}$ and its inverse to $\left(\frac{\partial \overline{x}^i}{\partial x^j}\right)_{i,j}$. We should have for instance:

$$G_x = P^T \overline{G}_x P = P^T I_n P \text{ and } {P^{-1}}^T G_x P^{-1} = I_n$$

The matrix $P^{-1} = \begin{bmatrix} \frac{v_1}{\sqrt{\lambda_1}} & \cdots & \frac{v_n}{\sqrt{\lambda_n}} \end{bmatrix}$ with v_i the eigenvector of G_x associated with the eigenvalue λ_i satisfies this equation (the family is chosen to be orthonormal for the ambient Euclidean metric: $v_i^T v_j = \delta_{i,j}$). Note that this gives us

$$P = \begin{bmatrix} \sqrt{\lambda_1} v_1^T \\ \vdots \\ \sqrt{\lambda_n} v_n^T \end{bmatrix}.$$

Remark 6 *The pullback metric g_x is always degenerate in this problem. Indeed, the dimension of its image is strictly bounded by the number of classes of the given task*[6]*.*

To take this into account, if $d = \dim \operatorname{Im} G_x$, one can rewrite the metric in normal coordinates by:

$$\overline{G}_x = \begin{bmatrix} \boldsymbol{I}_d & \boldsymbol{0}_{d,n-d} \\ \boldsymbol{0}_{n-d,d} & \boldsymbol{0}_{n-d,n-d} \end{bmatrix}.$$

The transition matrix P^{-1} is equal to $\begin{bmatrix} \frac{v_1}{\sqrt{\lambda_1}} & \cdots & \frac{v_d}{\sqrt{\lambda_d}} & v_{d+1} & \cdots & v_n \end{bmatrix}$.

Proposition 4.3 *If w is a solution to S2P, then there exists a scalar $\lambda \geq 0$ such that*

$$\left(P^T B P - \lambda I_n\right) w = \lambda v \tag{4}$$

with $B = I_n + \frac{1}{3} R_v$.

Proof Using again the KKT conditions but with the constraint $\|v + w\|_2^2 = \left\|v + P^{-1}\overline{w}\right\|_2^2 \leq \varepsilon^2$, it implies that there exists a scalar $\lambda \geq 0$ such that:

$$\begin{aligned} &\nabla_{\overline{w}} \left(\|\overline{w}\|_2^2 + \frac{1}{3} \overline{w}^T R_v \overline{w} \right) \\ &\quad - \lambda \nabla_{\overline{w}} \left(\left\|v + P^{-1}\overline{w}\right\|_2^2 - \varepsilon^2 \right) = 0 \\ \Longrightarrow\ &\overline{w} + \frac{1}{3} R_v \overline{w} - \lambda \left({P^{-1}}^T \left(P^{-1}\overline{w} + v \right) \right) = 0. \end{aligned}$$

Thus

$$\begin{aligned} &P^T \left(I_n + \frac{1}{3} R_v \right) P w = \lambda \left(w + v \right) \\ \Longleftrightarrow\ &P^T \left(B - \lambda {P^{-1}}^T P^{-1} \right) P w = \lambda v \\ \Longleftrightarrow\ &\left(P^T B P - \lambda I_n \right) w = \lambda v \end{aligned}$$

where $B = I_n + \frac{1}{3} R_v$. ∎

6. See Grementieri and Fioresi (2021) for the proof.

Corollary 4.4 *In normal coordinates, Equation 4 rewrites as:*

$$PP^T B\overline{w} = \lambda\left(\overline{w} + \overline{v}\right) \;\; ie \;\; \left(PP^T B - \lambda I_n\right)\overline{w} = \lambda\overline{v}.$$

Remark 7 *Note that* $PP^T = \mathrm{diag}\left(\lambda_i\right)$.

Corollary 4.5 *Whenever* λ *is not an eigenvalue of* $P^T BP$, $\left(P^T BP - \lambda I_n\right)$ *is non-singular and*

$$w = \lambda\left(P^T BP - \lambda I_n\right)^{-1} v. \tag{5}$$

It remains to find a λ such that the constraint $\|w+v\|_2^2 \leq \varepsilon^2$ is satisfied. There are two cases:

1. either $\|w+v\|_2^2 = \varepsilon^2$ and $\lambda > 0$,
2. or $\|w+v\|_2^2 < \varepsilon^2$ and $\lambda = 0$.

4.1 The case $\lambda > 0$

We will use the constraint $\|w+v\|_2^2 = \varepsilon^2$ to get λ. We suppose in what follows that 2λ is not an eigenvalue of B, ie $(2\lambda - 1)$ is not an eigenvalue of $\frac{1}{3}R_v$. The constraint may be written as:

$$\begin{aligned}\|w+v\|_2^2 &= \left\|\lambda\left(P^T BP - \lambda I_n\right)^{-1} v + v\right\|_2^2 \\ &= \left\|\left(\lambda\left(P^T BP - \lambda I_n\right)^{-1} + I_n\right) v\right\|_2^2.\end{aligned}$$

Lemma 4.6

$$\lambda\left(P^T BP - \lambda I_n\right)^{-1} + I_n = \left(P^T BP - \lambda I_n\right)^{-1} P^T BP.$$

Proof

$$\begin{aligned}&\left(P^T BP - \lambda I_n\right)\left(\lambda\left(P^T BP - \lambda I_n\right)^{-1} + I_n\right) \\ =&\lambda\left(P^T BP - \lambda I_n\right)\left(P^T BP - \lambda I_n\right)^{-1} + \left(P^T BP - \lambda I_n\right) \\ =&\cancel{\lambda I_n} + P^T BP - \cancel{\lambda I_n} = P^T BP.\end{aligned}$$

■

Thus,

$$\varepsilon^2 = \|w+v\|_2^2 = \left\|P^T BP\left(P^T BP - \lambda I_n\right)^{-1} v\right\|_2^2. \tag{6}$$

To find λ that satisfies Equation 6, we will study the vanishing points of:

$$\begin{array}{rccl}\varphi & : & [0,\infty[& \longrightarrow & [0,\infty[\\ & & \lambda & \longmapsto & \left\|P^T BP\left(P^T BP - \lambda I_n\right)^{-1} v\right\|_2^2 - \varepsilon^2\end{array}$$

However, finding the vanishing points of such a function is not an easy task. Several methods may be used. A numerical method such as the Newton's method Dennis and Schnabel (1996) could be applied.

Alternatively, observe that problem S2P can be simplified by using the triangular inequality to get back to an easier eigenvalue problem. Indeed, consider the following problem:

$$\max_{w} \|w\|_{\mathcal{X}}^2 \text{ subject to } \begin{cases} \|w\|_2 \leq \varepsilon - \mu \\ \|v\|_2^2 = \mu^2 < \varepsilon^2 \\ v \text{ eigenvector of } G_x \end{cases} \tag{S2.2P}$$

This new problem is illustrated on Figure 3. The green circle is the true budget and the two other smaller circles represent the triangular inequality approximation. One can see that the second step w does not reach the green circle but stop before due to the approximation.

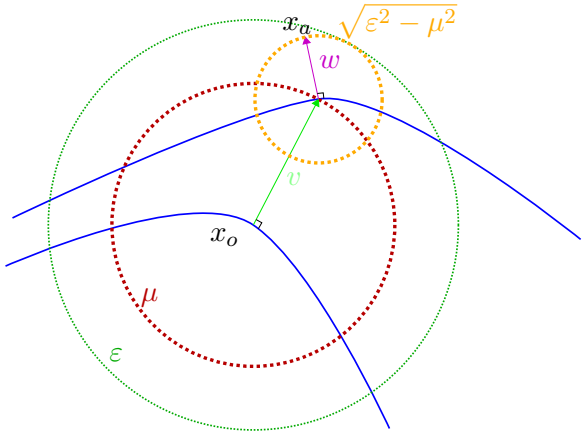

Figure 3: The two-step attack in action with the triangular inequality simplification. The three circles represent the Euclidean budget. The blue curves represent the leaves of the kernel foliation.

Proposition 4.7 *Any solution of S2.2P problem will satisfy the constraint of S2P problem.*

Proof Indeed, by the triangular inequality, $\|w + v\|_2 \leq \|w\|_2 + \|v\|_2 \leq (\varepsilon - \mu) + \mu = \varepsilon$. ■

With this new constraint, KKT's conditions boil down to

$$P^T B P w = \lambda w$$

or in normal coordinates:

$$P P^T B \overline{w} = \lambda \overline{w}.$$

Proposition 4.8 *A solution to S2.2P is to choose $\overline{w}$ to be the eigenvector of PP^TB with the highest eigenvalue λ and with the appropriate Euclidean norm of $\varepsilon - \mu$.*

4.2 The case $\lambda = 0$

In that case, w is in the interior of the boundary of the problem. The problem reduces to

$$B\overline{w} = 0 \iff R_v\overline{w} = -3\overline{w}.$$

This means that w is the optimal second step if $\overline{w} \in \operatorname{Ker} B$, ie if w is eigenvector of R_v with eigenvalue -3. However, this case does not produce any interesting KKT admissible point. Indeed,

$$\|w\|_{\mathcal{X}}^2 = \|\overline{w}\|_2^2 + \frac{1}{3}\overline{w}^T R_v \overline{w} = \|\overline{w}\|_2^2 - \overline{w}^T\overline{w} = 0.$$

Therefore, the case $\lambda = 0$ does not lead to useful adversarial attacks when the previous approximations are applied to the problem. The study of this singularity is left as future work.

5. An enlightening play-test example

5.1 Setup

In this section, we focus on a low dimensional example in order to visualize more easily the effect of curvature on the efficiency of the adversarial attack. A simple neural network N_θ with one hidden layer of k neurons and sigmoids as activation functions is used. Its architecture is depicted on Figure 4.

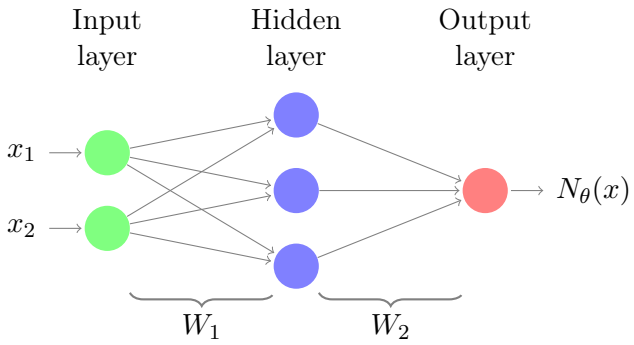

Figure 4: XorNet N_θ with 3 hidden neurons.

To be more precise, if $\sigma : a \in \mathbb{R}^d \mapsto \left(\frac{1}{1+e^{-a_i}}\right)_{i=1}^d \in \mathbb{R}^d$ is the sigmoid function and if $x \in \mathbb{R}^2$, $W_1 \in \mathcal{M}_{2,k}(\mathbb{R})$, $W_2 \in \mathcal{M}_{k,1}(\mathbb{R})$, we have

$$N_\theta(x) = \sigma\left(W_2\sigma\left(W_1 x + b_1\right) + b_2\right). \tag{7}$$

This neural network is then trained to approximate the very simple function `Xor`: $\{0,1\}^2 \to \{0,1\}$ defined in Table 1.

The output $N_\theta(x)$ is seen as the parameter p of a Bernoulli law and associates to the network the following probability distribution: $p(y \mid x, \theta)$ where θ is the vector containing the weights and biases $(W_i,\ b_i)$, x is the input and y is the true label.

Proposition 5.1 *The random variable $Y \mid X, \theta$ follows Bernoulli's law of parameter $p = N_\theta(x)$.*

Table 1: `Xor` function.

`Xor`	0	1
0	0	1
1	1	0

5.2 Computing the output FIM

The output of the network is the manifold of Bernoulli probability densities parameterized by the open segment $]0,1[$.

Proposition 5.2 *Let $p \in]0,1[$ and G_p the Fisher Information Metric at the point p.*

$$G_p = \frac{1}{p}\frac{1}{1-p} \tag{8}$$

Proof

$$\begin{aligned}
G_p &= -\mathbb{E}_{y|x,\theta}\left[\partial_p^2 \left(\ln P(y \mid x, \theta)\right)\right] \\
&= -\mathbb{E}\left[\partial_p^2 \left(y \ln p + (1-y)\ln\left(1-p\right)\right)\right] \\
&= -\mathbb{E}\left[\partial_p \left(\frac{y}{p} - \frac{(1-y)}{1-p}\right)\right] \\
&= -\mathbb{E}\left[-\frac{y}{p^2} - \frac{(1-y)}{(1-p)^2}\right] \\
&= \frac{1}{p} + \frac{1}{1-p} = \frac{1}{p}\frac{1}{1-p}.
\end{aligned}$$

■

5.3 Computing the pullback metric

Let $x \in \mathcal{M}$ be a point associated with p by the network.

Lemma 5.3 *The Fisher Information Metric G_x on $\mathcal{X}$ is the pullback metric of G_p by the neural network N_θ.*

Corollary 5.4 *If $J = \left[\frac{\partial p}{\partial x_j}\right]_{j=1,2} = \left[\frac{\partial N_\theta(x)}{\partial x_1} \quad \frac{\partial N_\theta(x)}{\partial x_2}\right]$, then*

$$G_x = J^T G_p J. \tag{9}$$

Remark 8 *The Jacobian matrix of a neural network J is not difficult to compute thanks to automatic differentiation available in most neural network training software's packages. Besides, this approach for computing J numerically allows the sequel of the article to stay quite general regarding the architecture of the neural network.*

Knowing how to compute the metric at any point unlocks the computation of the local method seen in Section 3 and the two-step method seen in Section 4 when the FIM is recomputed at the intermediary point. Additionally, studying the curvature of the input space is insightful to understand the behavior of the correction step in the two-step attack, and more generally to understand why adversarial attacks are, in some cases, so efficient.

Nonetheless, the pullback metric being almost always only semi-definite for machine learning tasks, it makes sense to consider its kernel. The curvature will have a decomposition term on the kernel of g and a decomposition term on its orthogonal[7]. To craft the attack, the orthogonal term will be the only curvature component of interest as stated at the end of Section 2.1. Thus in the following subsection, we compute the metric kernel for this neural network.

5.4 The metric kernel foliation

Definition 3 *The kernel of a metric G at the point x is defined by*

$$\ker_x G = \left\{ X \in T_p\mathcal{M} \mid X^T G_x Y = 0,\ \forall Y \in T_p\mathcal{M} \right\}.$$

This kernel defines an integrable distribution when Frœbenius' condition[8] is satisfied, and with this distribution emerges a Riemannian foliation on the input manifold, foliation defined by the action of the neural network.

Lemma 5.5 $\ker_x G = \ker J$.

Proof We omit $\frac{1}{p}\frac{1}{1-p}$ during the proof because it is always non-zero.

- Let us prove first that $\ker_x G \subset \ker J$. If $X \in \ker_x G$, then $X^T J^T J X = 0$. Hence $(JX)^T (JX) = 0$, or written otherwise: $\|JX\| = 0$. Hence $JX = 0$ and $X \in \ker J$.
- Then we can prove that $\ker J \subset \ker_x G$. This inclusion is simply due to the fact that if $X \in \ker J$, we have for all $Y \in T_p\mathcal{M}$ that $X^T J^T J Y = \underbrace{(JX)^T}_{=0} JX = 0$.

■

Proposition 5.6 *If at least one of the two components of J is non-zero, the distribution at x is one dimensional and given by $P_x = \mathrm{Span}\left(J_2(x)\partial_1 - J_1(x)\partial_2\right)$.*

Remark 9 *If $J = 0$, the leaf at x is singular and is of dimension 2.*

With the `Xor` function, the dimension of the leaves is 1, thus the condition of Frœbenius is trivially satisfied and P is integrable.

7. Here, the Euclidean orthogonal is considered.
8. For more details, see Chapter 1 of Molino (1988)

Proposition 5.7 *If $\gamma : t \in I \mapsto \gamma(t) \in \mathcal{M}$ is an integral curve for the distribution P, it satisfies the following ODE:*

$$\begin{aligned}\gamma'(t) &= J_2(\gamma(t))\,\partial_1 - J_1(\gamma(t))\,\partial_2 \\ &= J_{\gamma(t)} \begin{bmatrix} 0 & -1 \\ 1 & 0 \end{bmatrix}.\end{aligned}$$

It can be solved numerically quite easily with a finite difference method[9]. Figure 5 provides illustrations of the computed neural network kernel foliation with such a method for the `Xor` function (Figure 5a), and for the `Or` function (Figure 5b).

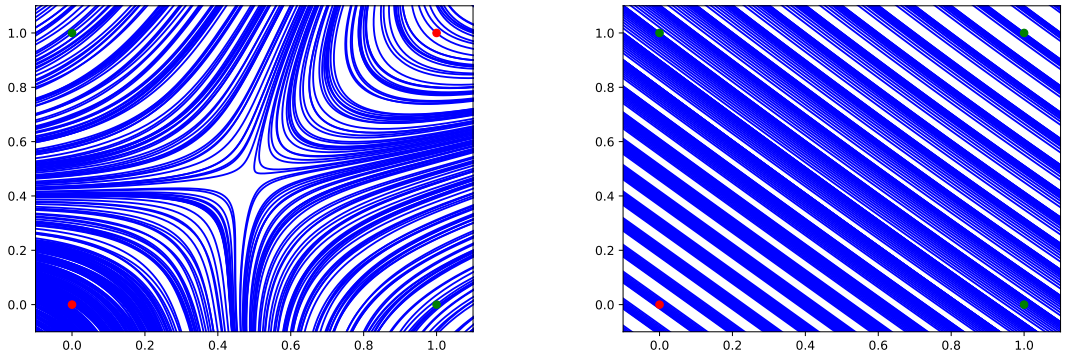

(a) Task: `Xor` (b) Task: `or`

Figure 5: Kernel foliation: the leaves are represented by the blue lines, the red dots are the 0 result and the green dots are the 1 results.

Remark 10 *For readability, the transverse leaves are not represented but can be easily deduced from figure 5 as Euclidean orthogonal curves to the blue ones.*

These results are quite interesting. First of all, we notice that a linearly separable problem such as the `or` function seems to have hyperplanes as leaves. In fact, it is easy to show that if the neural network is replaced by a linear form $x \mapsto \langle n, x\rangle + b$, then the leaves are hyperplanes defined by the normal vector n.

Second of all, one can see that there is a singular point close to the middle point $(0.5, 0.5)$ for the `Xor` task. Clearly, it is also easy to see that around that central point, the curvature of the leaves is the highest. Since the two-step adversarial attack makes use of the curvature, we can conjecture that it is in the central region that the second step will have the most impact. This phenomenon will be confirmed in Section 6.

5.5 Visualizing the curvature

In this section, we are computing the extrinsic curvature of a transverse leaf to see where the two-step attack will differ the most from the one-step attack. But first, we compute the

9. See for example Strikwerda (2004).

Levi-Civita connection. In the following of the article, we will use $i, j, k, l \in \{1, \ldots, \dim \mathcal{X}\}$ as indices and we will use the Einstein summation notation.

Definition 4 (Levi-Civita connection) *In coordinates e_i, if Γ_{ij}^k are Chrystoffel's symbols, then the Levi-Civita connection is defined by:*

$$\mathring{\nabla}_{e_j} e_i = \Gamma_{ij}^k e_k \quad .$$

Definition 5 (Riemannian curvature) *The* Riemannian Curvature Tensor *R is defined such that for all three tensor fields X, Y, Z,*

$$R(X,Y)Z = \nabla_X \nabla_Y Z - \nabla_Y \nabla_X Z - \nabla_{[X,Y]} Z.$$

In local coordinates, this gives:

$$\begin{aligned} R_{ijk}^l &= dx^l \left(R\left(\partial_i, \partial_j\right) \partial_k \right) \\ &= dx^l \left(\nabla_{\partial_i} \nabla_{\partial_j} \partial_k - \nabla_{\partial_j} \nabla_{\partial_i} \partial_k - \nabla_{[\partial_i, \partial_j]} \partial_k \right) \\ &= \frac{\partial \Gamma_{kj}^l}{\partial x^i} - \frac{\partial \Gamma_{ki}^l}{\partial x^j} + \Gamma_{kj}^\alpha \Gamma_{\alpha i}^l - \Gamma_{ki}^\alpha \Gamma_{\alpha j}^l. \end{aligned}$$

Remark 11 *In normal coordinates, at the origin point, one has:*

$$R_{ijkl} = \frac{1}{2} \left(\partial_i \partial_l g_{jk} + \partial_j \partial_k g_{il} - \partial_i \partial_k g_{jl} - \partial_j \partial_l g_{ik} \right).$$

Finding an explicit form for R is unreasonable, but since we are in the simpler case where the dimension of the transverse leaves is 1, a quick approximation can do the trick. In fact, leaves are embedded submanifolds of the Euclidean space and the extrinsic curvature, i.e. the second fundamental form, can be computed as the rate of rotation of the normal vector.

To approximate the second step w of the two-step attack, we look at the rotation speed of the unit normal to the kernel leaf $\vec{n}$ when moved by an infinitesimal step dx. This infinitesimal step is taken in the direction of the transverse leaf, and is Euclidean. Since the rotation rate is approximated by finite difference, one can expect the angle variation to be very small. To ensure numerical stability, the usual procedure based on its cosine computation using inner product is replaced by one using the cross product. The next lemma gives the expression of the sine of the angle variation between two close positions on curve transverse to the $\ker g$ foliation.

Lemma 5.8 *If $\vec{n}_y$ is the normal to the kernel leaf at $y \in \mathcal{X}$, and if $\cdot \times \cdot$ is the cross product, then the infinitesimal variation of angle is*

$$|d\theta| = \arcsin\left(\|\vec{n}_x \times \vec{n}_{x+dx}\|_2 \right).$$

Please note that in the small angles approximation, the sine can be replaced by the angle itself, thus recovering the usual infinitesimal rotation representation as a cross product (this is in fact a Lie algebra representation in the usual sense).

To approximate the effect of the curvature during the Euclidean step v, one has to compute the rotation matrix R of angle $d\theta$:

$$R = \begin{bmatrix} \cos(d\theta) & -\sin(d\theta) \\ \sin(d\theta) & \cos(d\theta) \end{bmatrix}$$

Proposition 5.9 *If v is the first step, the approximated second step is given by $w = Rv$ and then re-normalized to get $\|w\|^2 + \|v\|^2 = \varepsilon^2$.*

The signed curvature $d\theta$ for the `Xor` problem can then be seen on Figure 6. One can see that the curvature is the highest in the middle, around the point $(0.5, 0.5)$, and also on the diagonals.

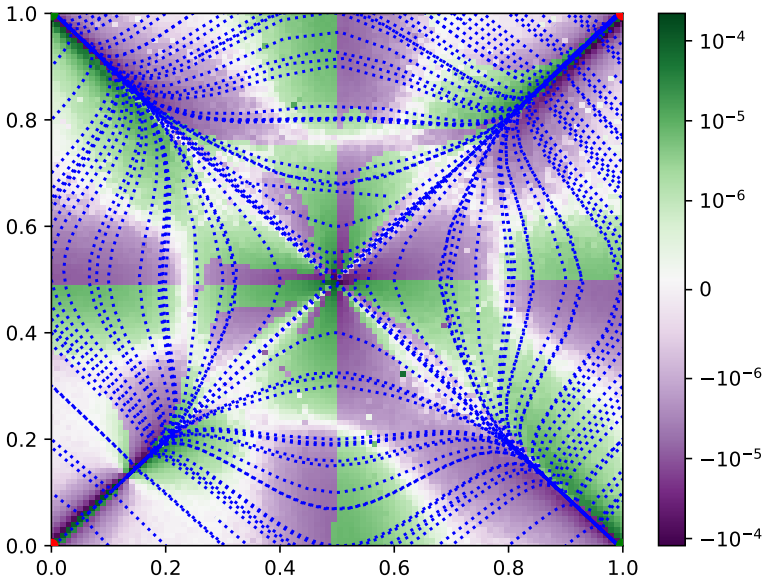

Figure 6: Extrinsic (signed) curvature of the transverse leaves ($d\theta$) for the task `Xor`, computed with a dx of 10^{-6}, with the transverse leaves in blue.

6. Numerical results

All codes used to produce the following results can be found in Tron.

6.1 Xor dataset

To compare the different attacks, we train a neural network with 8 hidden neurons on random points taken in the square $[0, 1]^2$ until convergence. We then compute the two different attacks which are the One Step Spectral Attack presented in Section 3 and the Two Step Spectral Attack presented at the beginning of Section 4 where we compute the FIM at x_o and $x_o + v$. These attacks are computed on 5000 random points selected in a square I of variable length. The fooling rate is then computed as the quotient of the number of fooled prediction by the total number of points. The budget is selected between 0 and 0.5. The first step in the two-step attacks is set to have Euclidean budget of 60% of the entire budget. We plot the results on Figure 7.

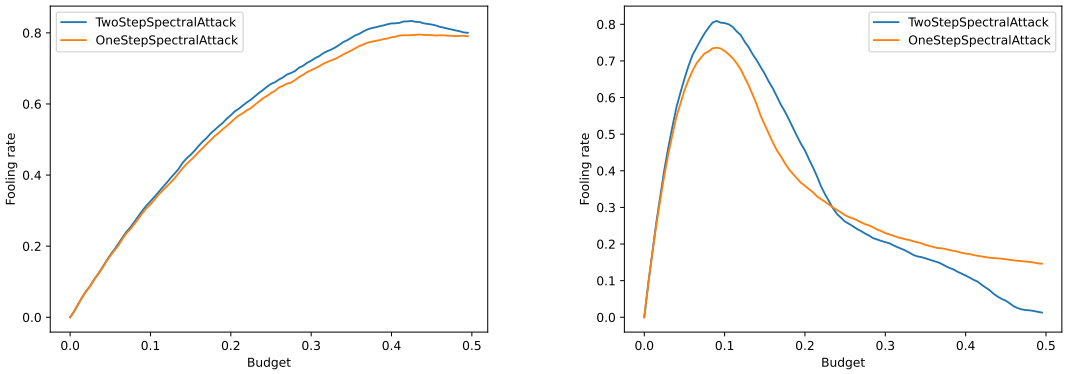

(a) $I = [0, 1]^2$ (b) $I = [0.4, 0.6]^2$

Figure 7: Fooling rates with respect to the Euclidean budget with random points taken in I for the task `Xor`.

On each figure, the two-step attack beats the one step attack (for reasonable budgets). The two-step attack is especially strong on the area where the curvature is the strongest: almost one point better for the TSSA at the peak in high curvature zones (see Figure 7b) compared to only half a point for the full space (see Figure 7a). Indeed, as seen on Figure 6, the curvature is really strong at the center of the square $[0, 1]^2$. The eigenvector of the FIM associated with the greatest eigenvalue is always orthogonal to the leaf kernel. Therefore, striking close to the middle region without taking into account the curvature usually results in not changing the output label: $(0, 0) \leftrightarrow (1, 1)$ or $(1, 0) \leftrightarrow (0, 1)$. This is why the TSSA gets better results by taking the curvature into account.

Remark 12 *Note that on Figure 7b, the fooling rates collapse shortly after budget* $= 0.1$ *because such high budgets makes every points leave the initial square* I*. These high budgets are too big for this area which is very close to the decision boundaries and the second step is not enough to compensate these instabilities, thus leading to such strange results at first glance.*

The illustration of the two different attacks can be found on Figure 8.

These results confirm our intuition that using the information of local curvature to craft an adversarial attack is meaningful. It also highlights the role of the leaves of the kernel foliation in the sensitivity of neural networks to attacks.

6.2 MNIST dataset

Next, we train a medium convolutional neural network with 4 layers (2 convolutional and 2 linear), `ReLU` as activation function and a `Softmax` function at the output. The fooling rates for the One Step Spectral Attack and the Two Step Spectral Attack are represented on Figure 9 for different Euclidean budget ranging from 0 to 10. The TSSA performs better than the OSSA, proving that curvature of the network is of interest in the construction of attacks or defenses to these attacks. The difference between the fooling rate of the TSSA

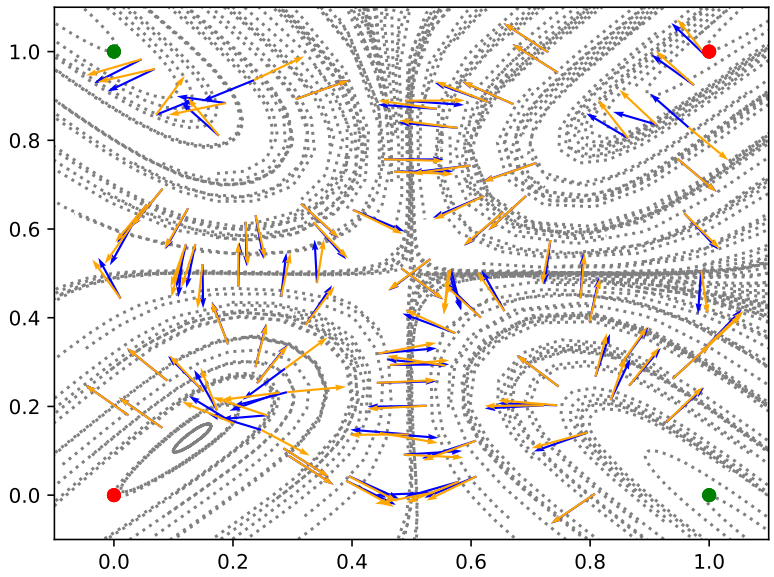

Figure 8: TSSA (in blue) compared to OSSA (in orange) with $\varepsilon = 0.1$. The kernel foliation is depicted with the grey lines.

and the fooling rate of the OSSA is plotted on Figure 10. It represents the advantage given by the curvature. As one can see, there are 3 different regimes:

1. The first one in blue is the region where the budget is small enough for the approximation $\exp_{x_o}(v) \approx x_o + v$ to hold. Taking into account the curvature does not modify enough the attack to fool the network on a lot of additional images compared to the straight line attack (OSSA).

2. The second regime in green is the region where the budget is high enough for the correction due to the curvature to be essential, and yet small enough for this same correction to hold. That is why the TSSA is much better than the OSSA for these budgets.

3. The third and last regime in red corresponds to budgets to big so that the approximations no longer make sense. At these horizons, the manifold is too non-linear.

Some examples of attacked images are also included for different budgets in order for the reader to realize that such small budgets are enough to fool the network while us - humans - still recognize very well the true digit. Other examples of attacks produced by the TSSA procedure are included in Figure 11 and in Figure 12 for different budgets.

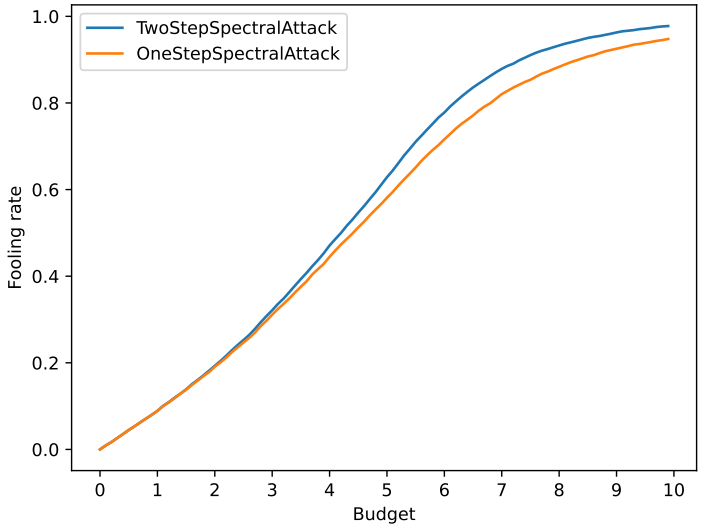

Figure 9: Fooling rates with respect to the Euclidean budget on all MNIST test-set.

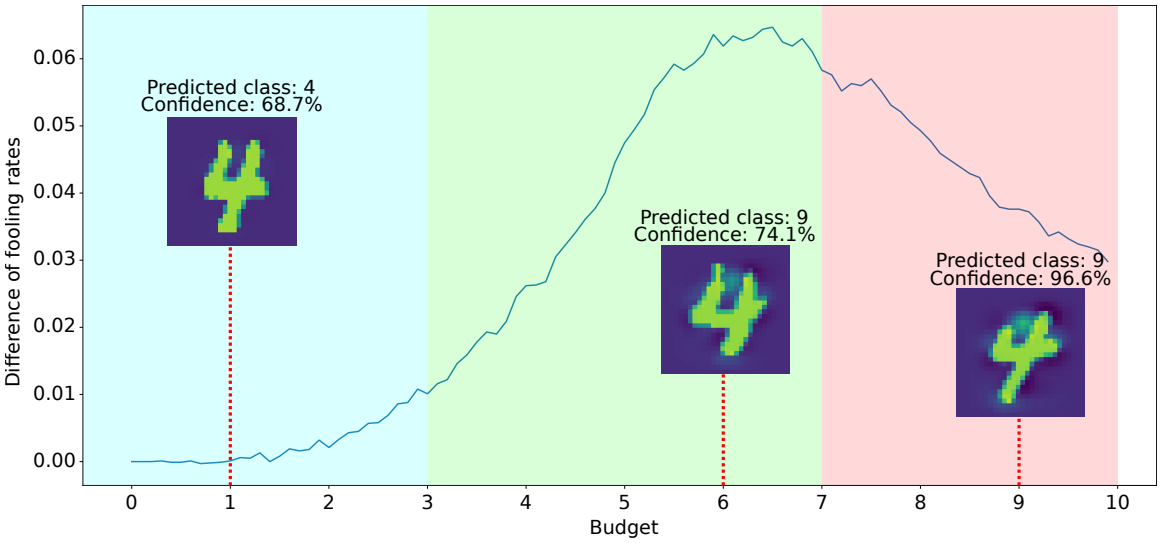

Figure 10: Difference between the fooling rate of the TSSA and the one of the OSSA with respect to the Euclidean budget, and some examples of the attacks it produces.

7. Conclusion

This paper explores the relationship between adversarial attacks and curvature of the data space. Using the curvature information, we have proposed a Two Steps Attack that achieves better results than the One Step Spectral Attack presented by Zhao et al. (2019). The analytical mathematical expression of the proposed attack explicitly uses the curvature tensor of the FIM kernel leaves. This emphasizes the importance of geometry in the construction

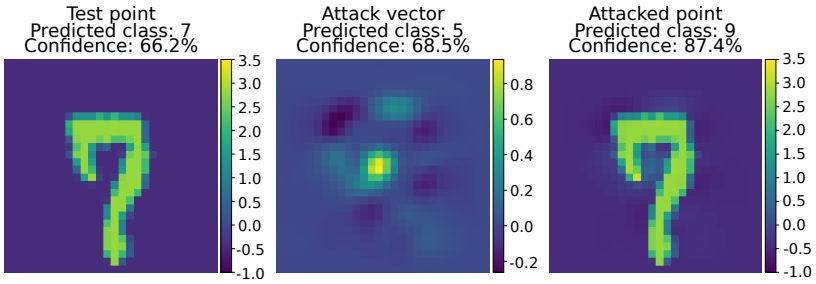

Figure 11: Result of the TSSA with a budget $\varepsilon = 3$.

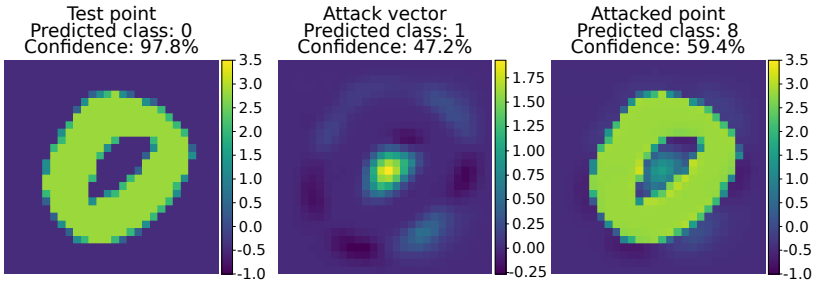

Figure 12: Result of the TSSA with a budget $\varepsilon = 7$.

of an efficient attack. Additionally, with simple experiments on a toy example, we have illustrated and confirmed that exploiting such geometrical information is relevant and actually outperforms a state of the art strategy. The mathematical construction of the proposed method opens also new opportunities for future research. Indeed, it is clear that, in the case of neural networks, the geometrical properties of the leaves of the kernel foliation is related to its robustness as explained above but more generally to its power to separate data points. Therefore, the geometry of the foliation is directly linked to the complexity of the model (i.e. the neural network architecture). A deeper analysis of these aspects should help in gaining knowledge and some explainability of the underlying principles at play in neural network learning and more generally deep learning methods. This will be the focus of our future research.

Acknowledgments

Our work has benefited from the AI Interdisciplinary Institute ANITI. ANITI is funded by the French "Investing for the Future - PIA3" program under the Grant agreement # ANR-19-PI3A-0004.

References

Shun-ichi Amari. *Information geometry and its applications*, volume 194. Springer, Tokyo, Japan, 2016.

Li Deng. The mnist database of handwritten digit images for machine learning research. *IEEE Signal Processing Magazine*, 29(6):141–142, 2012.

J. E. Dennis and Robert B. Schnabel. *Numerical Methods for Unconstrained Optimization and Nonlinear Equations*. Society for Industrial and Applied Mathematics, Philadelphia, PA, USA, 1996.

Alhussein Fawzi, Seyed-Mohsen Moosavi-Dezfooli, and Pascal Frossard. The robustness of deep networks: A geometrical perspective. *IEEE Signal Processing Magazine*, 34(6): 50–62, 2017.

Alhussein Fawzi, Hamza Fawzi, and Omar Fawzi. Adversarial vulnerability for any classifier. *Advances in neural information processing systems*, 31, 2018a.

Alhussein Fawzi, Omar Fawzi, and Pascal Frossard. Analysis of classifiers' robustness to adversarial perturbations. *Machine Learning*, 107(3):481–508, 2018b.

Charles Fefferman, Sanjoy Mitter, and Hariharan Narayanan. Testing the manifold hypothesis. *J. Amer. Math. Soc.*, 29:983 – 1049, 2016.

Justin Gilmer, Luke Metz, Fartash Faghri, Samuel S. Schoenholz, Maithra Raghu, Martin Wattenberg, and Ian Goodfellow. Adversarial spheres, 2018.

Ian J. Goodfellow, Jonathon Shlens, and Christian Szegedy. Explaining and harnessing adversarial examples. In Yoshua Bengio and Yann LeCun, editors, *3rd International Conference on Learning Representations, ICLR 2015, San Diego, CA, USA, May 7-9, 2015, Conference Track Proceedings*, 2015.

Luca Grementieri and Rita Fioresi. Model-centric data manifold: The data through the eyes of the model, 2021.

A. W. Tucker H. W. Kuhn. Nonlinear programming. In *Proceedings of 2nd Berkeley Symposium*, volume 2, pages 481–492, Berkeley, CA, USA, 1951. University of California press.

Ryo Karakida, Shotaro Akaho, and Shun-ichi Amari. Universal statistics of fisher information in deep neural networks: Mean field approach. In Kamalika Chaudhuri and Masashi Sugiyama, editors, *Proceedings of the Twenty-Second International Conference on Artificial Intelligence and Statistics*, volume 89 of *Proceedings of Machine Learning Research*, pages 1032–1041, Cambridge, MA, USA, 16–18 Apr 2019. PMLR.

J. Zico Kolter and Eric Wong. Provable defenses against adversarial examples via the convex outer adversarial polytope. In *ICML*, 2018.

Alexey Kurakin, Ian Goodfellow, and Samy Bengio. Adversarial machine learning at scale, 2016.

Aleksander Madry, Aleksandar Makelov, Ludwig Schmidt, Dimitris Tsipras, and Adrian Vladu. Towards deep learning models resistant to adversarial attacks, 2019.

P. Molino. *Riemannian Foliations*. Progress in Mathematics. Birkhäuser Boston, MA, USA, 1988. ISBN 9783764333706.

S. Moosavi-Dezfooli, A. Fawzi, and P. Frossard. Deepfool: A simple and accurate method to fool deep neural networks. In *2016 IEEE Conference on Computer Vision and Pattern Recognition (CVPR)*, pages 2574–2582, Los Alamitos, CA, USA, jun 2016. IEEE Computer Society.

Frank Nielsen. An elementary introduction to information geometry. *Entropy*, 22(10):1100, Sep 2020. ISSN 1099-4300.

Aditi Raghunathan, Jacob Steinhardt, and Percy Liang. Certified defenses against adversarial examples, 2020.

Uri Shaham, Yutaro Yamada, and Sahand Negahban. Understanding adversarial training: Increasing local stability of supervised models through robust optimization. *Neurocomputing*, 307:195 – 204, 2018.

Chaomin Shen, Yaxin Peng, Guixu Zhang, and Jinsong Fan. Defending Against Adversarial Attacks by Suppressing the Largest Eigenvalue of Fisher Information Matrix, 2019.

John C. Strikwerda. *Finite Difference Schemes and Partial Differential Equations, Second Edition*. Society for Industrial and Applied Mathematics, Philadelphia, PA, USA, 2004.

C. Szegedy, W. Zaremba, I. Sutskever, J. Bruna, D. Erhan, and I. Goodfellow et al. Intriguing properties of neural networks. *International Conference on learning representations (ICLR)*, 2014.

Eliot Tron. CurvNetAttack. URL `https://github.com/eliot-tron/CurvNetAttack`.

Thomas James Willmore. *An introduction to differential geometry*. Courier Corporation, USA, 2013.

Chenxiao Zhao, P. Thomas Fletcher, Mixue Yu, Yaxin Peng, Guixu Zhang, and Chaomin Shen. The Adversarial Attack and Detection under the Fisher Information Metric. *Proceedings of the AAAI Conference on Artificial Intelligence*, 33:5869–5876, 2019. ISSN 2374-3468, 2159-5399.

A. Notions of Riemannian geometry

Let $\mathcal{M} = (M, g)$ be a real Riemannian manifold of dimension n.

Definition 6 (length of a path) *Let $\gamma : [0,1] \to M$ be a C^1 path. The* length *of γ, denoted $l(\gamma)$ is defined by*

$$l(\gamma) = \int_0^1 g\left(\gamma(t), \gamma'(t), \gamma'(t)\right)^{1/2} dt$$

Definition 7 (geodesic) *Let $p,\ q$ be two points of M. The C^1 path $\gamma : [0,1] \to M$ is said to be a* geodesic *between p and q if:*

$$\gamma(0) = p,\ \gamma(1) = q$$
$$l(\gamma) = \inf\left\{l(\theta),\ \theta \in C^1([0,1),\ M),\ \theta(0) = p,\ \theta(1) = q\right\}$$

Definition 8 (geodesic distance) *The length of a geodesic between p and q is called the* geodesic distance*, denoted $d(p,q)$.*

In what follows, the Levi-Civita connexion of $\mathcal{M}$ will be denoted $\overset{\circ}{\nabla}$.

Definition 9 *Let $\gamma : [0,1] \to M$ be a C^2 path. It it said to be a geodesic of $\overset{\circ}{\nabla}$ is, for each $t \in]0,1[$ the following holds:*

$$\overset{\circ}{\nabla}_{\dot\gamma(t)}\dot\gamma(t) = 0 \tag{10}$$

The differential equation 10 translates in local coordinates to:

$$\frac{\partial^2\gamma^k}{\partial t^2}(t) + \Gamma_{ij}^k(\gamma(t))\frac{\partial\gamma^i}{\partial t}(t)\frac{\partial\gamma^j}{\partial t}(t) = 0 \tag{11}$$

For an initial point $p = \gamma(0)$, Cauchy-Lipschitz theorem shows that ther is a unique local solution to Equation 10.

Proposition A.1 *Let $p \in M$. There exist $\varepsilon > 0$ such that for all $v \in T_pM$, $\|v\| < \varepsilon$, there exist a unique geodesic $\gamma : [0,1] \to M$ such that $\gamma(0) = p,\ \gamma'(0) = v$. The function which to such v associates $\gamma(1)$ with γ the geodesic of $\overset{\circ}{\nabla}$ such that $\gamma(0) = p,\ \gamma'(0) = v$ is called the* exponential map *and denoted* $\exp_p$.

Proposition A.2 *Let $v \in T_pM$, $\|v\| < \varepsilon$ and let $q = \exp_p(v)$. Then $\gamma : t \in [0,1] \mapsto \exp_p(tv)$ is a geodesic between p and q. Besides, $l(\gamma) = \|v\|$.*

Remark 13 *Note that $\|v\| = g(p; v, v)^{1/2}$ is the riemannian norm and not the Euclidean norm.*

Definition 10 *$d\exp_p(0) = Id$ and thus the exponential map is a local diffeomorphism. Around each point, $\exp_p$ defines a chart of M. The local coordinates we get are called the* normal coordinates *at p.*

Definition 11 (logarithm map) *Let $p \in M$ and $\varepsilon > 0$ such that the exponential map is defined in $B(0, \varepsilon)$. For all $q \in M$ such that $d(p, q) < \varepsilon$ we set:*

$$\log_p(q) = v, \ \exp_p v = q.$$

Remark 14 *One can compute the logarithm by solving the following differential system:*

$$\begin{cases} \frac{\partial^2 \gamma^k}{\partial t^2}(t) + \Gamma_{ij}^k(\gamma(t)) \frac{\partial \gamma^i}{\partial t}(t) \frac{\partial \gamma^j}{\partial t}(t) = 0 \\ \gamma(0) = p, \ \gamma(1) = q \end{cases} \tag{12}$$

Proposition A.3 *In normal coordinates at $p \in M$, geodesics with origin p are strait lines going through the origin.*

Definition 12 (parallel transport) *Let $v \in T_pM$ and $q = \exp_p x$. The geodesic between p and q is $\gamma : t \in [0, 1] \mapsto tx$ in normal coordinates. Besides, the linear differential equation:*

$$\mathring{\nabla}_{\dot{\gamma}(t)} X(t) = 0, \ X(0) = v$$

has a solution on $[0, 1]$ called the parallel transport *of v.*

Parallel transport allows to go from a tangent vector at $q = \exp_p x$ to a tangent vector at p.

B. Fisher Information Metric

An important question arising when dealing with Fisher information metric is to know when going in the converse direction is feasible: given a Riemannian manifold $(\mathcal{X}, g)$, is it possible to find a probability family such that g is exactly its Fisher information? This is exactly what is behind the next definition.

Definition 13 (Statistical model) *A statistical model for a Riemannian manifold $(\mathcal{X}, g)$ is a probability space $(\Omega, \mathcal{T}, P)$ such that:*

- *It exists a family of probabilities p_x, $x \in \mathcal{X}$, absolutely continuous with respect to P.*
- *For any $x \in X$:*

$$g_{ij}(x) = E_{p_x}\left[\partial_i \ln p_x \partial_j \ln p_x\right]$$

Remark 15 *When p_x is C^2 with support not depending on x and the conditions for exchanging derivative and expectation are satisfied, then:*

$$g_{ij}(x) = -E_{p_x}\left[\partial_{ij} \ln p_x\right]$$

In such a case, the metric g is Hessian.

In nearly all cases considered in machine learning, the metric g is only semi-definite. It thus makes sense to consider its kernel.

Definition 14 *Let g be a semi-definite metric on a manifold $\mathcal{X}$. A tangent vector $X \in T_x\mathcal{X}$ is said to belong to the kernel $\ker_x g$ of g_x if for any $Y \in T_x\mathcal{X}$, $g(X, Y) = 0$.*

Proposition B.1 *Let $(\mathcal{X}, g)$ be a connected manifold with g a semi-definite metric. If it exists a torsionless connection ∇ on $T\mathcal{X}$ such that $\nabla g = 0$, then the mapping $x \in \mathcal{X} \to \ker_x g$ defines an integrable distribution, denoted by $\ker g$.*

Proof It is clear that for any $x \in \mathcal{X}$, $\ker_x g$ is a linear subspace of $T_x\mathcal{X}$. Let X, Y, Z be vector fields such that $Y \in \ker g$. Then, since $\nabla g = 0$ by assumption:

$$X\left(g(Y,Z)\right) = g\left(\nabla_X Y, Z\right) + g\left(Y, \nabla_X Z\right)$$

Since $Y \in \ker g$:

$$X\left(g(Y,Z)\right) = 0 = g\left(\nabla_X Y, Z\right)$$

and so, for any X, $\nabla_X Y \in \ker g$. This proves that the parallel transport of a vector in $\ker g$ is a vector in $\ker g$. The dimension of $\ker g$ is thus constant. Now, if $X, Y \in \ker g$, by the above result and since ∇ has vanishing torsion: $[X, Y] = \nabla_X Y - \nabla_Y X \in \ker g$, proving that $\ker g$ is an integrable distribution. ■

Remark 16 *If the dimension of $\ker g$ is not constant, then no torsionless connection ∇ can be such that $\nabla g = 0$. However, there is still a singular foliation associated with $\ker g$, with a canonical stratification by the dimension of $\ker g$.*

Proposition B.2 *Under the assumptions of prop. B.1, g defines a transverse metric for the $\ker g$ foliation.*

Proof This is essentially prop 3.2, p. 78 in Molino (1988). ■

The leaves of the $\ker g$ foliation are neutral submanifolds for the fisher information metric, that is moving along them will not modify the output distribution. On the other hand, the transverse metric is a measure of output variation when moving in a direction normal to the leaves.